Characterization of scattering losses in tapered optical fibers perturbed by a microfiber tip

Pengfei Zhang,[1,2,*] **Xin Wang,**[1] **Lijun Song,**[1] **Chenxi Wang,**[1] **Gang Li,**[1,2] **and Tiancai Zhang**[1,2]

[1]State Key Laboratory of Quantum Optics and Quantum Optics Devices, Institute of Opto-Electronics, Shanxi University, Taiyuan 030006, China
[2]Collaborative Innovation Center of Extreme Optics, Shanxi University, Taiyuan, Shanxi 030006, China
*Corresponding author: zhangpengfei@sxu.edu.cn

We demonstrate the characterization of the exponential-decay scattering losses in a tapered optical fiber (TOF) based on near-field-probe-induced scattering. A hemispherical microfiber tip (MFT) with a diameter of 37.3 µm is immersed into the evanescent field of a TOF and induces scattering losses of the TOF. The near-field scattering losses perturbed by the MFT depend on the distance between the MFT and the TOF. The MFT can elongate the penetration depth of the evanescent field significantly when the TOF diameter is small because the effective refractive index outside the TOF is changed by the MFT. The relationship between the scattering loss and the TOF-MFT distance is measured experimentally and is in good agreement with the numerical simulations. The lengthened evanescent field of the TOF can sense the multifarious matter on a substrate which is farther from the TOF sensitively.   © 2020 Optical Society of America

1. INTRODUCTION

Nanoscale photonic structures have attracted increasing attention in recent years due to their fascinating capability to guide intense evanescent fields at subwavelength scales. Therefore, nanoscale photonic structures have been a particularly versatile platform for applications including optical sensing [1], quantum optics [2], and quantum information processing [3].

Tapered optical fibers (TOFs), as a class of nanoscale photonic structures, have been a topic of great interest in recent years [4–8]. TOFs are fabricated by heating and stretching a regular single-mode fiber, where the regular single-mode fiber is narrowed down to a subwavelength diameter [9,10]. Evanescent fields are localized at the interface between the TOF with a high refractive index and air with a low refractive index. The evanescent fields are enhanced dramatically due to the small size of the TOF [11]. Therefore, the enhanced evanescent fields are confined strongly in the vicinity of the TOF surface, which can enhance the interface between evanescent fields and matter such as neutral atoms [12,13], color centers in diamond [14], quantum dots [15], molecules [16], metals [17,18], and graphene [19]. When the evanescent field of a TOF is particularly strong, it can be used to trap particles [20]. A promising and significant approach employed to trap atom arrays has been proposed and demonstrated experimentally using an optical dipole trap formed by a blue- and red-detuned nanofiber-guided evanescent field, called a two-color trap [21–23], which can extend

the interaction time and enhance the interface. TOFs with evanescent fields allow efficient coupling with other photonic structures, including near-lossless coupling between a TOF and a resonator [24,25] and coupling to photonic crystal resonators by combining a TOF and a nanofabricated grating [26]. Because TOF evanescent fields with a proper diameter can reach a significant proportion of the propagating mode, TOFs are very sensitive to environmental changes near the surface of the TOFs. Therefore, TOFs can play a key role in optical sensing applications [6].

The field intensity distributions of TOF evanescent fields can be described using Maxwell's equations and boundary conditions. The exact solutions can be obtained analytically [11]. The field strength drops off exponentially away from the TOF surface. Total internal reflection microscopy (TIRM) and scanning near-field optical microscopy (SNOM) are two significant techniques used to characterize the evanescent fields generated by a traditional scheme for applications in biology and optics [27–31]. In a traditional scheme, a laser beam is totally internally reflected at an interface between a prism with a high refractive index and air with a low refractive index. The evanescent fields extend into the air over a subwavelength distance. Both of these techniques commonly use expensive microscopes. The TIRM technique is used to measure evanescent fields directly by means of inserting microspheres into the evanescent fields [28] or coating a polymer on the interface [29], which will

affect the interface destructively and increase the experimental complexity. A near-field small-aperture probe is inserted into the evanescent field for the SNOM technique, which can also be used to measure the enhanced evanescent fields of integrated waveguides [32]. The probe disturbs the evanescent field distribution by multiple scattering between the probe and the surface [33]. How far the TOF evanescent fields can extend depends on the refractive index of the fiber core and cladding sensitively. The probe near the TOF surface can change the effective refractive index of the fiber cladding; therefore, the probe can modify the penetration depth of TOF evanescent fields.

In this paper, we propose and demonstrate the characterization of the scattering losses of a TOF directly based on near-field-probe-induced scattering. We use a hemispherical microfiber tip (MFT) measuring tens of micrometers as the near-field probe. The probe immerses into the evanescent field of the TOF and strongly changes the effective refractive index of the fiber cladding, at the same time the MFT induces TOF scattering losses. The effective refractive index of the cladding increases when the TOF-MFT distance decreases. The penetration depth of TOF evanescent fields is modified when the MFT is close enough to the TOF and the scattering loss depends on the TOF-MFT distance. The relationship between the scattering loss and the TOF-MFT distance can be characterized experimentally. The scattering loss in such a TOF-MFT system can be precisely simulated by the three-dimensional (3D) finite difference time-domain (FDTD) method [34]. We compare experimental data and FDTD simulated results of the scattering loss versus the distance between the MFT and the TOF, and we find that the scattering loss versus TOF-MFT distance is in good agreement with the simulations. The TOF diameters can be estimated based on the technique described in Ref. [34]. This method of characterizing the scattering losses of TOFs has great potential for detecting small particles or multifarious matter on a substrate and also for applications for chemistry or biology.

2. EXPERIMENTS AND SIMULATIONS

We consider a TOF with a subwavelength diameter and a hemispherical MFT perpendicular to the TOF. A schematic of this proposal is shown in Fig. 1(a). The energy proportion of the evanescent field outside the TOF with a subwavelength diameter is considerable. If the MFT with a refractive index of 1.45 is immersed in the evanescent field of the TOF and the MFT will increase the effective refractive index of the cladding. Thus we set the effective refractive index of the MFT-changed cladding as 1.3 and we theoretically plot the electric-field intensity distribution along the x axis of the fundamental HE_{11} mode [34] for TOF diameters of 382, 613, and 965 nm, which is shown in Fig. 1(b). The guided-mode vacuum wavelength is 852 nm. The blue shadow represents a TOF with a refractive index of 1.45. The polarization of the guided mode is along the x axis. From Fig. 1(b), it can be seen that a strong evanescent field extends into the surrounding air, and the field decreases exponentially along the x axis. The penetration depth of the evanescent field
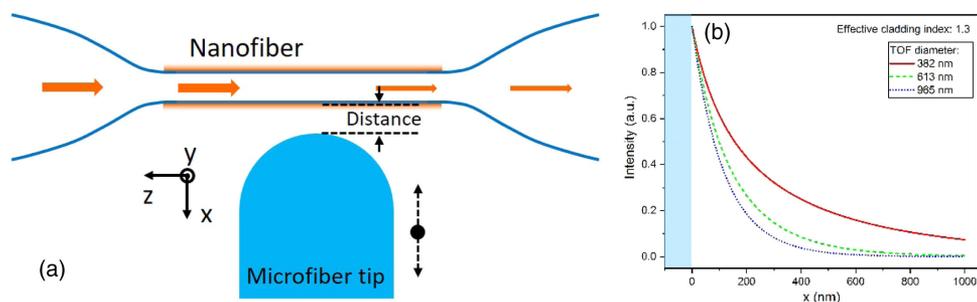

Fig. 1. (a) Schematic of the TOF-MFT system. The figure is not drawn to scale. (b) Electric-field intensity distribution of the TOF along the x axis of the fundamental HE11 mode for TOF diameters of 382, 613, and 965 nm when the effective refractive index of the cladding is 1.3. The vacuum wavelength of the guided mode is 852 nm. The polarization of the guided mode is along the x axis.
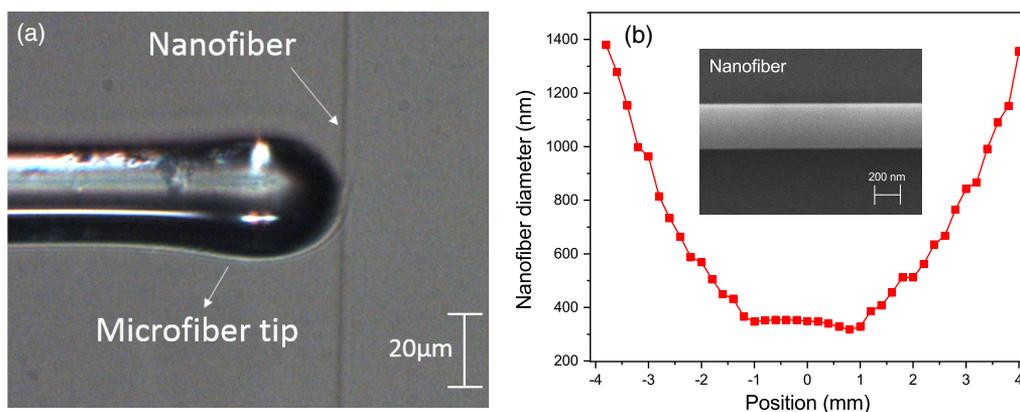

Fig. 2. (a) Camera image of the MFT-TOF system. (b) TOF diameter as a function of position along the TOF axis. The inset shows a typical SEM image of a nanofiber.

can be increased with decreasing TOF diameter for the same effective refractive index of the MFT-changed cladding.

The camera image of the experimental setup for characterizing the scattering losses of TOFs perturbed by a microfiber tip is shown in Fig. 2(a). A laser beam is collimated and coupled into an optical single-mode fiber by a fiber coupler. The vacuum wavelength of the laser is 852 nm. The laser beam passes through a TOF, and the power of the output is measured by a detector. The TOF is fabricated from a single-mode fiber (SM800, Fibercore) by the flame-brush method [9]. The hemispherical MFT used in our experiments is fabricated by a CO_2 laser. The details of the fabrication setup and procedures for the TOFs and MFTs are discussed in Ref. [34]. The diameter of the MFT is 37.3 µm, and the MFT is utilized in the following experiments. The MFT is positioned on a three-axis piezo stage with nanometer resolution (P-611.3 NanoCube XYZ Piezo Stage, Physik Instrumente). The length of the MFT is less than 1 mm relative to where it is anchored. The setup is kept inside a two-layer glass cover to avoid the influence of air currents and dust. The MFT can be controlled precisely to be immersed into the evanescent field of the TOF. The distance between the TOF and MFT can be controlled with a high spatial resolution up to 10 nm. Figure 2(b) shows the TOF diameter measured by scanning electron microscopy (SEM) as a function of position along the TOF axis, and the inset shows a typical SEM image of the TOF.

To determine the MFT-induced scattering loss, we first measured the transmitted power P_1 of the TOF for different distances between the TOF and the MFT. Second, we measured the transmitted power P_2 without the MFT. Finally, we obtained the scattering loss $L = 1 - T = 1 - P_1/P_2$. Owing to the much larger size of the MFT compared to the nanofiber, the method is robust with respect to the alignment of the MFT to the nanofiber along the axis perpendicular to the nanofiber. We moved the MFT along the axis of the TOF to measure the scattering loss versus the TOF-MFT distance for various TOF diameters from 382 nm to 965 nm and a fixed wavelength of 852 nm. The TOF diameters are estimated based on the technique described in Ref. [34]. MFTs with large diameters can be fabricated easily. The diameters can be measured precisely using an optical microscope, and the spherical tip shape indicates that the scattering loss is insensitive to alignment imperfections.

The experimental results of scattering losses versus TOF-MFT distance are shown in Fig. 3(a) (red circles). For various TOF diameters, each scattering loss curve is normalized with respect to the maximum scatting loss. We use the 3D-FDTD method (Lumerical Solutions, Inc.) to numerically simulate the scattering loss as a function of the TOF-MFT distance. We used the software to build the model of the MFT and the TOF. The model sizes are determined by the measured values of the microfiber tip using a CCD camera and SEM. The simulation results are shown in Fig. 3(a) by black solid lines. For the numerical simulation, we calculate an average of the two cases for the x- and y-polarizations of the guided modes. The reason is that the guided mode polarizations in the TOF have a small effect on the scattering loss when the MFT is close to the surface of the TOF [34]. The simulation results for these two cases show a small difference. For this reason, we use a rotated polarization for our experiments. We present the averaged curves for the x- and y-polarizations in Fig. 3(a). The experimental results can be

statistically compared to the FDTD numerical simulations. The deviation between the experimental results and FDTD simulation is derived from (i) the TOF-MFT distance fluctuations
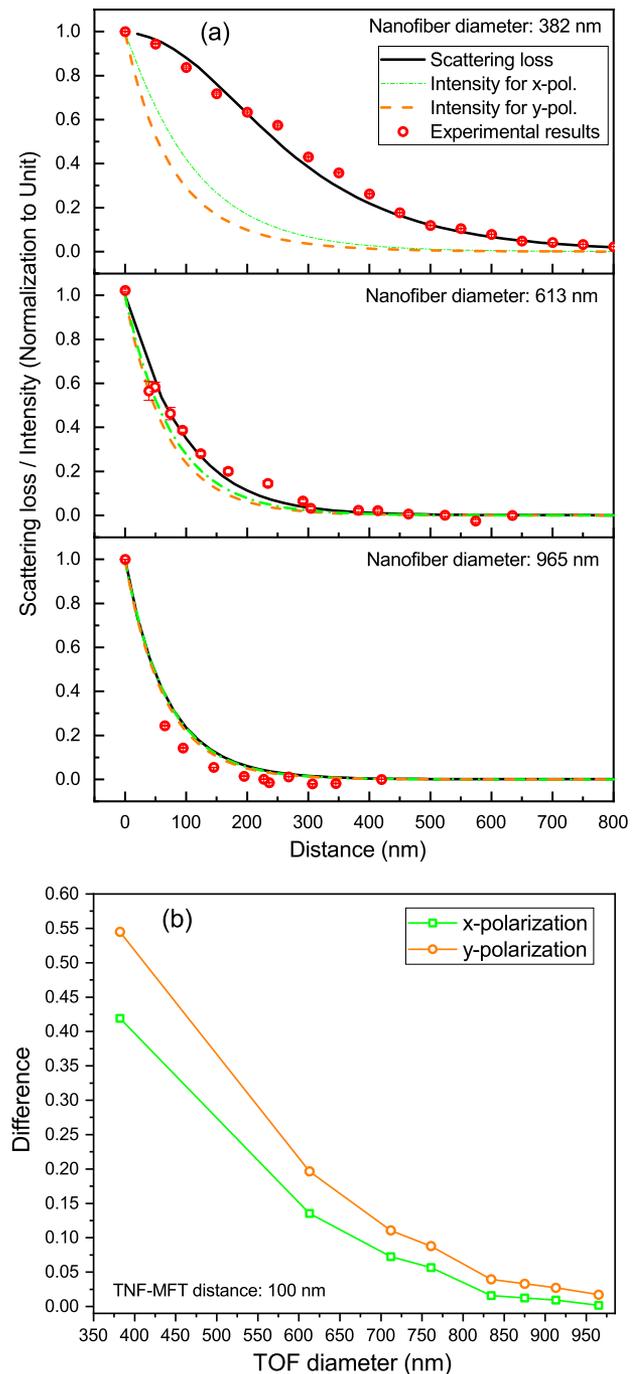

Fig. 3. (a) Scattering loss of the TOF caused by the MFT and evanescent field intensity of the TOF as a function of the distance between the TOF and the MFT for different TOF diameters from 382 nm to 965 nm. The vacuum wavelength of the guided mode is 852 nm, and the MFT diameter is 37.3 µm. The orange dashed lines and green dashed–dotted lines are the evanescent field intensity of the TOF for the x- and y-polarizations, respectively. The black solid lines are the FDTD numerical simulation results, and the red circles are the experimental data. (b) Differences between the scattering loss and the evanescent field intensity for the x- and y-polarizations (green squares and orange circles) as a function of the TOF diameter with a fixed TOF-MFT distance of 100 nm.
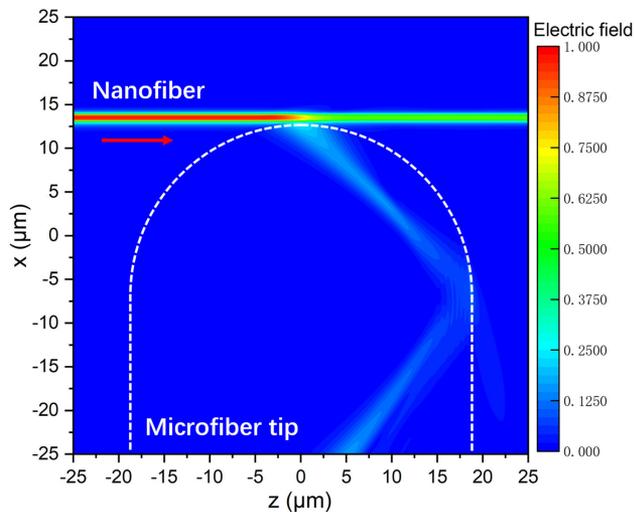
Fig. 4.   Electric field distribution in the x–z plane. The TOF diameter is 382 nm and the TOF- MFT distance is 240 nm.

due to mechanical vibrations, (ii) controlling the spatial resolution of the stage for the MFT, (iii) the polarization of the guided mode, and (iv) the fluctuations of the optical power. In addition, we plot the electric-field intensity distributions of the TOF for the x-polarization (orange dashed lines) and y-polarization (green dashed–dotted lines) for comparison. The intensity distributions are normalized with respect to the intensities on the surface of the TOF. For thinner TOF with the diameter of 382 nm, the distance which can cause scattering loss is bigger than the penetration depth of the evanescent field with cladding of air. The MFT can cause significant scattering losses when the MFT is just immersed into the evanescent field. This means the MFT increases the effective cladding index. As the TOF-MFT distance decreases, the effective cladding index increases and the penetration depth of the evanescent field increases, which is consistent with the theoretical prediction in Fig. 1(b). In this case, the scattering loss depends on the overlap area between the modified evanescent field and the MFT. When the MFT is moved to be closer to the TOF, the penetration depth of evanescent fields increases more and the MFT can cause more scattering loss. For thicker TOF, the effect of the MFT on the penetration depth of the evanescent field reduces. There is not any distinct increment of the penetration depth for a TOF diameter of 965 nm. We conclude the differences between the simulated scattering loss and the evanescent field intensity for the x- and y-polarizations as a function of the TOF diameter and plot the differences in Fig. 3(b). The TOF-MFT distance is fixed at 100 nm. This behavior can be understood as the energy proportion of the evanescent field decreasing when the TOF diameter increases. Thus, the perturbative effect of the MFT on the evanescent field intensity reduces. The penetration depth of the evanescent field increases with decreasing TOF diameter, which is predicted theoretically as shown in Fig. 1(b). The overlap between the MFT and the evanescent field causes less scattering losses for thicker TOF.

To show how the scattering happens when the TOF is close to the MFT, we simulate and plot the electric field distribution in the x–z plane, shown in Fig. 4. The light is guided by the nanofiber and propagates from left to right. The red arrow in Fig. 4 shows the direction of the light. The TOF diameter is 382 nm and the TOF-MFT distance is 240 nm. The light is scattered by the MFT and a part of the light is coupled into the MFT, which can be seen clearly. While the other part of the light is scattered to the free space, which cannot be seen in Fig. 4. The light is weaker after the scattering due to the MFT.

3. SUMMARY

In conclusion, we have demonstrated a method to characterize the scattering losses in a TOF based on near-field-probe-induced scattering. The exponential decay of scattering losses perturbed by a MFT can be measured by this method. Experimentally, a MFT with a hemispherical diameter of 37.3 μm is utilized as a near-field probe which can induce the scattering losses of the TOF. The MFT near the TOF can affect the effective refractive index outside the TOF and extend the penetration depth of the evanescent fields when the TOF diameter is small enough. The numerical simulations are in good agreement with the experimental results. The effect of the MFT for the TOF with a larger size becomes weaker. The TOF-MFT system can elongate the penetration depth of the mode outside the TOF, which can be used to detect the photons from the emitters on a substrate conveniently. Therefore, our convenient and simple approach could be used for applications based on TOF evanescent fields, including evanescently coupled with photonic structures, offering a convenient technique for sensing the multifarious matter on a substrate which is farther from the TOF sensitively for the applications in chemistry or biology.

Disclosures.   The authors declare no conflicts of interest.

REFERENCES

1. I. R. Matias, S. Ikezawa, and J. Corres, *Fiber Optic Sensors* (Springer, 2017).
2. I. D'Amico, D. G. Angelakis, F. Bussieres, H. Caglayan, C. Couteau, T. Durt, B. Kolaric, P. Maletinsky, W. Pfeiffer, P. Rabl, A. Xuereb, and M. Agioy, "Nanoscale quantum optics," Riv. Nuovo Cimento **42**, 153–195 (2019).
3. B. Gouraud, D. Maxein, A. Nicolas, O. Morin, and J. Laurat, "Demonstration of a memory for tightly guided light in an optical nanofiber," Phys. Rev. Lett. **114**, 180503 (2015).
4. L. Tong and M. Sumetsky, *Subwavelength and Nanometer Diameter Optical Fibers* (Zhejiang University\Springer, 2017).
5. K. P. Nayak, M. Sadgrove, R. Yalla, F. L. Kien, and K. Hakuta, "Nanofiber quantum photonics," J. Opt. **20**, 073001 (2018).
6. L. Tong, F. Zi, X. Guo, and J. Lou, "Optical microfibers and nanofibers: atutorial," Opt. Commun. **285**, 4641–4647 (2012).
7. X. Wu and L. Tong, "Optical microfibers and nanofibers," Nanophotonics **2**, 407–428 (2013).

8. P. Solano, J. A. Grover, J. E. Hoffman, S. Ravets, F. K. Fatemi, L. A. Orozco, and L. R. Steven, "Optical nanofibers: a new platform for quantum optics," Adv. At. Mol. Opt. Phys. **66**, 439–505 (2017).

9. T. A. Birks and Y. W. Li, "The shape of fiber tapers," J. Lightwave Technol. **10**, 432–438 (1992).

10. L. Tong, R. R. Gattass, J. B. Ashcom, S. He, J. Lou, M. Shen, I. Maxwell, and E. Mazur, "Subwavelengthdiameter silica wires for low-loss optical wave guiding," Nature **426**, 816–819 (2003).

11. F. Le Kien, J. Q. Liang, K. Hakuta, and V. I. Balykin, "Field intensity distributions and polarization orientations in a vacuum-clad subwavelength-diameter optical fiber," Opt. Commun. **242**, 445–455 (2004).

12. K. P. Nayak, P. N. Melentiev, M. Morinaga, M. Fam Le Kien, V. I. Balykin, and K. Hakuta, "Optical nanofiber as an efficient tool for manipulating and probing atomic fluorescence," Opt. Express **15**, 5431–5438 (2007).

13. G. Sague, E. Vetsch, W. Alt, D. Meschede, and A. Rauschenbeutel, "Cold-atom physics using ultrathin optical fibers light-induced dipole forces and surface interactions," Phys. Rev. Lett. **99**, 163602 (2007).

14. L. Liebermeister, F. Petersen, A. V. Münchow, D. Burchardt, J. Hermelbracht, T. Tashima, A. W. Schell, O. Benson, T. Meinhardt, A. Krueger, A. Stiebeiner, A. Rauschenbeutel, H. Weinfurter, and M. Weber, "Tapered fiber coupling of single photons emitted by a deterministically positioned single nitrogen vacancy center," Appl. Phys. Lett. **104**, 031101 (2014).

15. R. Yalla, F. Le Kien, M. Morinaga, and K. Hakuta, "Efficient channeling of fluorescence photons from single quantum dots into guided modes of optical nanofiber," Phys. Rev. Lett. **109**, 063602 (2012).

16. F. Warken, E. Vetsch, D. Meschede, M. Sokolowski, and A. Rauschenbeutel, "Ultra-sensitive surface absorption spectroscopy using sub-wavelength diameter optical fibers," Opt. Express **15**, 11952 (2007).

17. J. Petersen, J. Volz, and A. Rauschenbeutel, "Chiral nanophotonic waveguide interface based on spin-orbit interaction of light," Science **346**, 67–71 (2014).

18. H. Wu, Q. Bao, X. Guo, D. Dai, and L. Tong, "Low-loss photonic-like guided mode in metal-supported optical nanofibers," Appl. Phys. Lett. **114**, 031104 (2019).

19. X. Wu, S. Yu, H. Yang, W. Li, X. Liu, and L. Tong, "Effective transfer of micron-size graphene to microfibers for photonic applications," Carbon **96**, 1114–1119 (2016).

20. G. Brambilla, G. Senthil Murugan, J. S. Wilkinson, and D. J. Richardson, "Optical manipulation of microspheres along a subwavelength optical wire," Opt. Lett. **32**, 3041–3043 (2007).

21. F. L. Kien, V. I. Balykin, and K. Hakuta, "Atom trap and waveguide using a two-color evanescent light field around a subwavelength-diameter optical fiber," Phys. Rev. A **70**, 063403 (2004).

22. E. Vetsch, D. Reitz, G. Sagué, R. Schmidt, S. T. Dawkins, and A. Rauschenbeutel, "Optical interface created by laser-cooled atoms trapped in the evanescent field surrounding an optical nanofiber," Phys. Rev. Lett. **104**, 203603 (2010).

23. A. Goban, K. S. Choi, D. J. Alton, D. Ding, C. Lacroûte, M. Pototschnig, T. Thiele, N. P. Stern, and H. J. Kimble, "Demonstration of a state-insensitive compensated nanofiber trap," Phys. Rev. Lett. **109**, 033603 (2012).

24. S. M. Spillane, T. J. Kippenberg, O. J. Painter, and K. J. Vahala, "Ideality in a fiber-taper-coupled microresonator system for application to cavity quantum electrodynamics," Phys. Rev. Lett. **91**, 043902 (2003).

25. F. Cheng, P. Zhang, X. Wang, and T. Zhang, "Experimental investigation on the coupling process between microtoroidal resonators and tapered nanofibers," J. Quantum Opt. **23**, 74–81 (2017).

26. M. Sadgrove, R. Yalla, K. P. Nayak, and K. Hakuta, "Photonic crystal nanofiber using an external grating," Opt. Lett. **38**, 2542–2545 (2013).

27. S. Harlepp, J. Roberta, N. C. Darnton, and D. Chatenay, "Subnanometric measurements of evanescent wave penetration depth using total internal reflection microscopy combined with fluorescent correlation spectroscopy," Appl. Phys. Lett. **85**, 3917 (2004).

28. A. L. Mattheyses and D. Axelrod, "Direct measurement of the evanescent field profile produced by objective-based total internal reflection fluorescence," J. Biomed. Opt. **11**, 014006 (2006).

29. C. Niederauer, P. Blumhardt, J. Mücksch, M. Heymann, A. Lambacher, and P. Schwille, "Direct characterization of the evanescent field in objective-type total internal reflection fluorescence microscopy," Opt. Express **26**, 20492–20506 (2018).

30. E. Betzig and J. K. Trautman, "Near-field optics: microscopy, spectroscopy, and surface modification beyond the diffraction limit," Science **257**, 189–195 (1992).

31. T. Hong, J. Wang, T. Xu, and L. Sun, "Direct measurement of evanescent wave interference with a scanning near-field optical microscope," Chin. Phys. Lett. **21**, 907 (2004).

32. J. Hahn, C. E. Rüter, F. Fecher, J. Petter, D. Kip, and T. Tschudi, "Measurement of the enhanced evanescent fields of integrated waveguides for optical near-field sensing," Appl. Opt. **47**, 2357–2360 (2008).

33. Y. Kawata, T. Okamoto, and W. Inami, "Non-perturbative measurement of evanescent fields," Opt. Commun. **410**, 30–34 (2018).

34. P. Zhang, F. Cheng, X. Wang, L. Song, C.-L. Zou, G. Li, and T. Zhang, "Nondestructive measurement of nanofiber diameters using microfiber tip," Opt. Express **26**, 31500–31509 (2018).